

# Drip instabilities of continental lithosphere: acceleration and entrainment by damage

Karen Paczkowski,<sup>1</sup> David Bercovici,<sup>1</sup> William Landuyt<sup>2</sup> and Mark T. Brandon<sup>1</sup>

<sup>1</sup>Department of Geology and Geophysics, Yale University, P.O. Box 208109, New Haven, CT 06520-8109, USA. E-mail: karen.paczkowski@yale.edu

<sup>2</sup>ExxonMobil Exploration Company, P.O. Box 4778, Houston, TX 77210-4778, USA

Accepted 2012 January 27. Received 2012 January 13; in original form 2011 July 8

## SUMMARY

Geological evidence indicates large-volume lithospheric drip instabilities form under regions of continental lithosphere. The size of these drips suggests that either the base of the lithosphere is volumetrically increased or the highly viscous upper lithosphere participates in the drip. Previous theoretical models using simple rheologies have been unable to produce unforced large-volume drip instabilities. Thus large drip instabilities are typically induced by thickening or destabilizing the mobile base of the lithosphere through tectonic forcing, such as convergent thickening or dense magmatic emplacement following extension. Here, we propose a theory of lithospheric drip instabilities that may arise naturally from the thermal and rheological structure of Earth, independent of specific tectonic forcings. Using damage physics relevant for Earth, we find a large portion of the lithosphere may be mobilized and entrained into growing drip instabilities. For a critical amount of damage, the growth is accelerated sufficiently that large-volume drip instabilities may form within geologically feasible time-frames. We therefore suggest large-volume lithospheric drip instabilities may arise independently of tectonic settings through damage-assisted mobilization and entrainment of the highly viscous lithosphere.

**Key words:** Instability analysis; Dynamics of lithosphere and mantle; Mechanics, theory, and modelling; Rheology: crust and lithosphere; Rheology: mantle.

## 1 INTRODUCTION

Lithospheric drips are thought to cause intraplate removal of mantle–lithosphere material by gravitational convective instabilities. Perturbations to the lithosphere–mantle interface grow due to the negative buoyancy of the lithosphere, but must overcome viscous resistance of the mantle and lithosphere as well as thermal diffusion. Seismic, compositional, structural and isotopic data suggest that large volume lithospheric drip instabilities form in a variety of tectonic settings such as the Tibetan Plateau (Houseman *et al.* 1981; England & Houseman 1988, 1989), the Altiplano Plateau in the central Andes (Ghosh *et al.* 2006a,b; Garzzone *et al.* 2006; Rowley & Garzzone 2007; Garzzone *et al.* 2008; Hoke & Garzzone 2008), the Sierra Nevada Mountain Range (Humphreys & Clayton 1990; Jones *et al.* 1994; Saleeby & Foster 2004; Boyd *et al.* 2004; Zandt *et al.* 2004; Yang & Forsyth 2006; Ducea & Saleeby 1996; Saleeby *et al.* 2003), and the Great Basin (West *et al.* 2009). In basic physical models (Houseman & McKenzie 1982; Yuen & Fleitout 1985; Buck & Parmentier 1986; Dumoulin *et al.* 2001; Huang *et al.* 2003; Korenaga & Jordan 2003; Dumoulin *et al.* 2005), small volume second-scale convective instabilities arise from the hot, mobile, yet gravitationally unstable, base of the lithosphere. However, under the continental lithosphere, the large volume of the observed drips with diameters of 80–200 km and extending to depths of 100–500 km (Zandt *et al.* 2004; West *et al.* 2009) suggest either the mobile base of the lithosphere has been volumetrically thickened, or the highly

viscous upper lithosphere is somehow included in the drip. Basic temperature dependent rheologies of the lithosphere seem to preclude the possibility of colder, stiffer lithosphere being included in drip instabilities, while non-Newtonian power-law rheology can completely inhibit the formation of drip instabilities (Houseman & Molnar 2001). Therefore many models invoke specific tectonic settings, such as convergence induced thickening or dense magma emplacement, to increase the volume of the mobile base of the lithosphere. The subsequent removal of the volumetrically thickened lithospheric base is then used to explain the large volume of the observed drips. Here, we revisit the possibility that large-volume lithospheric drips may form through mobilization of the highly viscous lithosphere by including a weakening, damage mechanism relevant for Earth. By allowing the highly viscous lithosphere to participate in the growing drip instability we propose a generalized theory, independent of tectonic setting, for the formation of large-volume lithospheric drips as naturally arising features of the thermal and rheological structure of Earth.

Large volume lithospheric drip instabilities were first proposed to explain geological data suggesting sudden uplift of the Tibetan Plateau (Houseman *et al.* 1981; England & Houseman 1988, 1989). Although the timing and rate of the surface uplift of Tibet is still debated, geological data have suggested the Tibetan Plateau experienced uplift (Molnar *et al.* 1993) followed by a transition from convergent (McKenzie & Sclater 1971; Molnar & Tapponnier 1975; Molnar *et al.* 1981; Patriat & Achache 1984; Chang *et al.* 1986;

Lin & Watts 1988) to extensional (Molnar & Tapponnier 1975; Tapponnier *et al.* 1981; Chen & Molnar 1983; Armijo *et al.* 1986) tectonics. Various authors (England & Houseman 1989) have suggested that as the lithosphere thickens through convergence and thermal cooling, its negative buoyancy overcomes diffusive smoothing and the viscous resistance of the lithosphere and mantle, forming a large-volume lithospheric drip instability. The detachment of the drip may induce surface uplift of a few kilometres and a potential energy increase (per unit surface area of lithosphere) of  $5\text{--}10 \times 10^{12} \text{ N m}^{-1}$  as the system readjusts to isostatic equilibrium (England & Houseman 1989). The potential energy increase caused by the large-volume drip instability and subsequent uplift effectively acts as an additional pressure term in the system, increasing the vertical compressive stresses, which changes the relative magnitude of the three principal stresses in the system, thus shifting the region from a compressional to an extensional tectonic regime (England & Houseman 1989).

In the case of the Tibetan Plateau, recent palaeoaltimetry isotopic data indicates that the surface uplift need not be rapid (Rowley & Garzione 2007; Murphy *et al.* 2009). However, this same isotopic method also provides robust evidence for the loss of a large-volume lithospheric drip under the Altiplano Plateau in the central Andes (Garzione *et al.* 2006; Ghosh *et al.* 2006a,b; Rowley & Garzione 2007; Hoke & Garzione 2008; Garzione *et al.* 2008). Stable isotope palaeoelevation data from oxygen isotopes (Garzione *et al.* 2006) and clumped  $\text{CO}_2$  isotope  $\Delta_{47}$  palaeothermometry (Ghosh *et al.* 2006b) indicate the Altiplano Plateau experienced 2.5–3.7 km of rapid uplift between 10 and 6.8 Ma. This rapid uplift is induced by the loss of the dense thickened lower lithosphere through a large-volume drip instability formed during convergence (Garzione *et al.* 2006; Ghosh *et al.* 2006a,b; Rowley & Garzione 2007; Hoke & Garzione 2008; Garzione *et al.* 2008).

In addition, seismic (Humphreys & Clayton 1990; Jones *et al.* 1994; Saleeby & Foster 2004; Boyd *et al.* 2004; Zandt *et al.* 2004; Yang & Forsyth 2006; West *et al.* 2009) and compositional (Ducea & Saleeby 1996; Saleeby *et al.* 2003) studies have also detected large volume lithospheric drip instabilities. Tomographic evidence from the Sierra Nevada Mountain Range indicates an isostatically thin crust ( $\sim 35$  km) (Jones *et al.* 1994) overlying a large detached region of dense lithosphere (Yang & Forsyth 2006). The large-volume drip beneath the Sierra Nevada Mountain Range is also thought to form as a result of convergence induced thickening. The data suggest that the thick lithospheric root detached and dripped into the mantle producing a seismically fast zone separated from the lithosphere. A compositional shift in xenolith source material between 10 and 3 Ma further implies that the seismically fast zone is of lithospheric origin (Ducea & Saleeby 1996; Saleeby *et al.* 2003). Older xenoliths ( $\sim 10$  Ma) consist of dense eclogitic lithosphere derived assemblages, while younger xenoliths ( $\sim 3$  Ma) are comprised of peridotitic upper mantle assemblages (Ducea & Saleeby 1996; Saleeby *et al.* 2003). Such a compositional shift is expected if the dense eclogitic root drips off and is replaced by the upper mantle peridotite between the occurrence of these two xenolith types.

Seismic shear wave splitting and  $P$  wave tomographic models suggest the formation of another large-volume drip instability beneath the Great Basin (West *et al.* 2009). LPO data indicates a direction of mantle flow corresponding to the direction of plate motion in regions surrounding the Great Basin, but a lack of LPO fabric under the Great Basin. This lack of anisotropy under the Great Basin could be a result of vertically downward mantle flow in the region caused by the formation of a drip instability. Tomographic models image a large-volume velocity anomaly of cold, dense material

under the Great Basin, suggesting a single large-volume drip is driving the downward flow. However, the Great Basin is an extensional tectonic region, suggesting that convergence induced thickening is not responsible for triggering the large-volume drip instability. The drip instability is instead postulated to have been induced by the emplacement of dense material at the base of the lithosphere, such as a magmatic pulse frozen as eclogite or having left a residual dense mafic cumulate, which has subsequently detached.

The volume of the drip instabilities beneath both the Sierra Nevada Mountain Range and the Great Basin have been estimated from seismic data to have radii of 80–200 km and depth extents of 100–500 km (Zandt *et al.* 2004; West *et al.* 2009). The large volume of the drips does not arise naturally using Rayleigh-Bénard convection models due to the temperature dependence of the viscosity, which prohibits a large portion of the cold, dense lithosphere from becoming entrained in the drip instability. Furthermore, Houseman & Molnar (2001) found that the addition of non-Newtonian power-law rheology further suppresses the development of drip instabilities, requiring the initial perturbation amplitude to have a significant finite amplitude, most likely resulting from horizontal tectonic shortening. Considerable advancements have been made to model the rheological behaviour of Earth beyond these simple temperature dependent and non-Newtonian power-law rheologies (Tackley 2000; Bercovici *et al.* 2000; Bercovici 2003), but few of these results have been applied to study second scale convective features, such as lithospheric drip instabilities. Instead, most drip models force instabilities by increasing the volume of the mobile base of the lithosphere through convergence induced thickening (Houseman *et al.* 1981; Platt & England 1993; Houseman & Molnar 1997; Conrad 2000; Conrad & Molnar 1997; Molnar *et al.* 1998; Lev & Hager 2008) or dense magma emplacement (Elkins-Tanton & Hager 2000; Jull & Kelemen 2001; West *et al.* 2009), whichever is most appropriate for the regional tectonics where the large-volume drip has been detected. These arguments assume that only the hot, lower lithosphere can be mobilized and entrained in the growing drip. However, the large volume of these drips can also be explained by mobilization and entrainment of the cold, highly viscous, upper lithosphere. Entrainment of the upper lithosphere requires localized weakening to penetrate further into the lithosphere and accelerate the instabilities enough for large volume drips to form within geologically feasible timeframes.

Here we develop a general theory for the development of lithospheric drip instabilities by using a damage mechanism consistent with tectonic plate generation on Earth and thus capable of weakening the highly viscous parts of the lithosphere (Bercovici *et al.* 2001a,b; Bercovici & Ricard 2003, 2005; Landuyt *et al.* 2008; Landuyt & Bercovici 2009). Damage induced weakening helps mobilize and entrain the highly viscous lithosphere into the growing drip, thus increasing the negative buoyancy of the drip and accelerating its growth such that large volume drips occur within geologically feasible timeframes. We determine the critical amount of damage necessary for large-volume lithospheric drip instabilities to form on Earth, and suggest lithospheric instabilities may form naturally from perturbations to the lithosphere–mantle interface without requiring special tectonic conditions or thickening of the lithosphere.

## 2 THEORY AND GOVERNING EQUATIONS

We investigate the formation of lithospheric instabilities as a function of the damage parameters. We model a gravitationally unstable

system, with a dense, cold, high viscosity lithosphere over-lying a less dense, hotter, low viscosity mantle. We approximate both the lithosphere and mantle as continuous viscous fluids, using Stoke's equations for creeping flow. Mass and momentum conservation under the Boussinesq approximation are therefore given by

$$\nabla \cdot \vec{v} = 0, \quad (1)$$

$$-\nabla \cdot (2\mu\dot{\epsilon}) + \nabla P + \rho\vec{g} = 0, \quad (2)$$

where  $\vec{v}$  is the velocity,  $\mu$  is the viscosity,  $\rho$  is the density,  $P$  is the pressure,  $\vec{g}$  is gravity and  $\dot{\epsilon}_{ij} = \frac{1}{2}(\partial v_i/\partial x_j + \partial v_j/\partial x_i)$  is the  $ij$ th component of the strain rate tensor.

To track the thermal evolution of the system, we use conservation of internal energy,

$$\frac{\partial T}{\partial t} + \vec{v} \cdot \nabla T = \kappa \nabla^2 T, \quad (3)$$

where  $T$  is the temperature,  $\kappa$  is the thermal diffusivity and  $t$  is time.

We introduce damage physics with a grain size dependent self-softening mechanism, which has been shown to produce tectonic plate like behaviour (Bercovici & Ricard 2005; Landuyt *et al.* 2008; Landuyt & Bercovici 2009), to investigate the formation and growth of lithospheric instabilities.

We assume viscosity is a function of fineness (i.e. inverse grain size),  $A$ , and the temperature-dependence of viscosity as given by the Frank-Kamenetskii approximation. The viscosity is therefore written as

$$\mu = \mu_{\max} \left( \frac{A}{A_0} \right)^{-m} \exp(-\theta T'), \quad (4)$$

where  $T' = (T - T_s)/\Delta T$ ,  $\Delta T = T_b - T_s$ ,  $T_s$  and  $T_b$  are the temperatures at the surface and base of the mantle,  $\theta = \ln(\bar{\mu})$  is the Frank-Kamenetskii parameter,  $\bar{\mu} = \mu_{\max}/\mu_{\min}$ ,  $\mu_{\max}$  and  $\mu_{\min}$  are the maximum and minimum initial viscosities in the system,  $A_0$  is the reference fineness and  $m$  is chosen for grain size dependent diffusion creep.

We assume there is an ensemble of grain sizes in our system, such that diffusion and dislocation are occurring simultaneously (Rozel *et al.* 2010). Damage therefore has a viscosity that is sensitive to grain size and grain size is allowed to evolve over time as a function of local stress and temperature conditions. Fineness is generated (i.e. grain size is reduced) by partitioning a fraction of the deformational work to surface energy used to 'damage' the material (Bercovici & Ricard 2005; Austin & Evans 2007). Fineness is reduced through surface-tension-driven grain growth. The phenomenological law governing fineness is given by the competition between these two processes (Landuyt *et al.* 2008),

$$\frac{DA}{Dt} = \frac{f}{\gamma} \Psi - kA^p, \quad (5)$$

where  $\Psi = \nabla \vec{v} : \underline{\sigma}$  is the viscous deformational work,  $\underline{\sigma}$  is the viscous stress tensor,  $f$  is the fraction of deformational work used to create new grain boundaries,  $\gamma$  is the grain boundary surface energy,  $k$  is the healing rate and  $p = 3$  is chosen to reproduce classical surface tension driven grain growth whereby the grain size increases with the square root of time (Karato 1989; Evans *et al.* 2001).

Due to the negative buoyancy of the lithosphere, perturbations to the lithosphere–mantle interface will grow over time. To examine the growth of lithospheric instabilities we perturb the lithosphere–mantle system and calculate the characteristic instability timescale  $\tau$ , defined as the time required for the perturbation to grow to half the thickness of the lithosphere, as a function of the damage parameters. We determine the rheological conditions that allow perturbations to the interface to grow into large-volume drips that entrain the highly viscous lithosphere and examine whether the formation of those drips is possible in geological timeframes.

### 3 AMPLITUDE ANALYSIS

#### 3.1 Model setup

Here, we develop a relationship between perturbation growth and the damage parameters to predict under what conditions large-volume lithospheric drip instability growth will occur. We track the amplitude  $h$  of the drip instability at the base of the lithosphere by tracking the evolution of the  $0.5\Delta T + T_s$  isotherm (Fig. 1). This isotherm is initially at depth  $H_0$ .

The temperature profile of the lithosphere is defined in terms of an error function as

$$T = \frac{0.5\Delta T}{\text{erf}(1)} \text{erf}\left(\frac{z}{H_0 + h_{\text{tot}}(x, t)}\right) + T_s, \quad (6)$$

where  $z$  is the depth and  $h_{\text{tot}}$  is the variation of the base of the lithosphere.  $h_{\text{tot}}$  is further divided into two components such that  $h_{\text{tot}}(x, t) = \tilde{h}(t) + h(x, t)$ , where  $\tilde{h}(t)$  is the change in the base of the lithosphere due to uniform half-space cooling and  $h(x, t)$  is the change in the base of the lithosphere due to a sinusoidal perturbation (Fig. 1).

Assuming horizontal temperature gradients are much smaller than vertical temperature gradients ( $\partial T/\partial x \ll \partial T/\partial z$ ) at the maximum amplitude of the growing drip instability, (3) becomes

$$\frac{\partial T}{\partial t} + w \frac{\partial T}{\partial z} = \kappa \nabla^2 T, \quad (7)$$

where  $w$  is the vertical velocity.

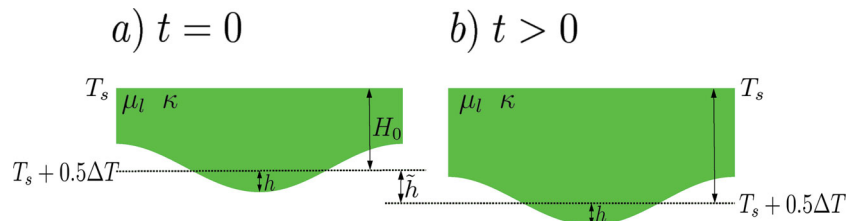


**Figure 1.** Schematic of the model for the amplitude analysis. The initial system (a) has the base of the lithosphere at depth  $H_0$ , which is defined by the isotherm  $0.5\Delta T + T_s$ , where  $\Delta T$  is the potential temperature drop across the full lithosphere–mantle system (Fig. 5a). At time  $t > 0$  (b), the perturbation height  $h$  has changed and the thickness of the lithosphere has increased by  $\tilde{h}$  due to thermal diffusion.  $\tilde{h}$  is governed by the cooling of a half space, thus increasing the lithospheric thickness  $H_0$  by  $\sim(\text{age})^{1/2}$ .

Substituting (6) into (7), evaluating at  $z = H_0 + h_{\text{tot}}$ , and solving for  $h_{\text{tot}}$  gives the evolution of the base of the lithosphere as

$$\frac{dh_{\text{tot}}}{dt} = w + \kappa \left( \frac{\partial^2 h_{\text{tot}}}{\partial x^2} + \frac{2}{H_0 + h_{\text{tot}}} \right). \quad (8)$$

We solve for  $w$  in terms of  $h$  by balancing the negatively buoyant stresses driving perturbation growth with the viscous stresses acting to resist deformation given as

$$\Delta \rho g h(x, t) = \sigma_{zz} \approx w \frac{\mu_l}{H_0}, \quad (9)$$

where  $\Delta \rho$  is the density contrast due to thermal contraction, which is set to correspond to  $\Delta \rho = \rho_l - \rho_m$ , the subscripts  $l$  and  $m$  refer to the lithosphere and mantle, and  $\sigma_{zz}$  is the non-hydrostatic vertical normal stress at the boundary. Assuming the halfspace cooling by itself is a solution to (8), we obtain a system of two coupled differential equations for  $h$  and  $\tilde{h}$  as

$$\begin{aligned} \frac{dh(x, t)}{dt} &= \frac{\Delta \rho g H_0}{\mu_l} h(x, t) + \kappa \left( \frac{\partial^2 h(x, t)}{\partial x^2} \right. \\ &\quad \left. + \frac{2}{H_0 + \tilde{h}(t) + h(x, t)} - \frac{2}{H_0 + \tilde{h}(t)} \right) \end{aligned} \quad (10)$$

$$\frac{\partial \tilde{h}(t)}{\partial t} = \frac{2\kappa}{H_0 + \tilde{h}(t)}. \quad (11)$$

Because the drip is entraining material from the entire lithosphere, not just the  $0.5\Delta T + T_s$  isotherm, for a conservative estimate of the viscous resistance in the system we evaluate (4) at the maximum model temperature,  $T_s$ , which results in

$$\mu_l = \mu_{\text{max}} \left( \frac{A}{A_0} \right)^{-m}. \quad (12)$$

We also assume the stresses in the system are entirely driven by the negative buoyancy of the growing perturbation, thus  $\Psi = (\Delta \rho g h)^2 / \mu_l$ . Fineness evolution (5) can then be approximated as

$$\frac{dA}{dt} = \frac{f}{\gamma} \frac{(\Delta \rho g h)^2}{\mu_l} - kA^p. \quad (13)$$

We substitute (12) into (10), (11) and (13) and non-dimensionalized by  $h = H_0 h'$ ,  $\tilde{h} = H_0 \tilde{h}'$ ,  $t = (\mu_{\text{max}} / \Delta \rho g H_0) t'$  and  $A = A_0 \mathcal{A}$ , and subsequently drop the primes to obtain

$$\frac{dh}{dt} = \mathcal{A}^m h + \frac{1}{\mathcal{R}} \left( \frac{d^2 h}{dx^2} + \frac{2}{1 + \tilde{h} + h} - \frac{2}{1 + \tilde{h}} \right) \quad (14)$$

$$\frac{d\tilde{h}}{dt} = \frac{1}{\mathcal{R}} \left( \frac{2}{1 + \tilde{h}} \right) \quad (15)$$

$$\frac{d\mathcal{A}}{dt} = \tilde{f} h^2 \mathcal{A}^m - \tilde{k} \mathcal{A}^p, \quad (16)$$

where here we introduce the local Rayleigh number of the system,  $\mathcal{R}$ , and the non-dimensional damage number,  $\tilde{f}$ , and healing rate,  $\tilde{k}$ , as

$$\mathcal{R} = \frac{\Delta \rho g H_0^3}{\kappa \mu_{\text{max}}} \quad (17)$$

$$\tilde{f} = \frac{\Delta \rho g H_0}{A_0 \gamma} f \quad (18)$$

$$\tilde{k} = \frac{A_0^{p-1} \mu_{\text{max}}}{\Delta \rho g H_0} k. \quad (19)$$

Assuming the perturbation has an initial amplitude  $h_0$  and a wavelength  $\lambda$ , the three coupled equations mentioned above are solved to determine the time evolution of the perturbation as a function of damage parameters. We calculate the characteristic instability timescale  $\tau$ , defined as the time at which the perturbation amplitude reaches  $0.5H_0$ .

## 3.2 Results

### 3.2.1 Newtonian rheology

First, we examine the case of a constant Newtonian lithospheric viscosity by setting  $\tilde{f} = \tilde{k} = 0$ . The lithospheric viscosity is set to  $\mu_{\text{max}} = 10^{25}$  Pa s to correspond to highly viscous but still ductile lithosphere, which must be mobilized and entrained in the drip instability for large-volume drip formation. We select the perturbation wavelength  $\lambda = 11.4H_0$  to correspond to the least stable mode, which is found in the linear stability analysis (Appendix A) for the initial viscosity ratio  $\bar{\mu} = 10^2$ . We set  $\mathcal{R} = 3.3$  by selecting  $H_0 = 320$  km,  $\kappa = 10^{-6} \text{ m}^2 \text{ s}^{-1}$ ,  $\Delta \rho = 100 \text{ kg m}^{-3}$  and set our initial conditions to be  $h = 0.05H_0$  and  $\tilde{h} = 0$ . We set  $m = 2$  for grain size dependent diffusion creep (Karato 1989) and  $p = 3$  to match experiments explained in Section 2. Using these parameters we integrate (14)–(16) and find  $\tau = 2$  billion years (Fig. 2). This timescale suggests a more complex rheological mechanism must be at work to produce lithospheric drip instabilities that entrain the highly viscous part of the lithosphere within geologically reasonable timeframes.

### 3.2.2 Cases with damage

We now set  $\tilde{f} \neq 0$  and  $\tilde{k} \neq 0$  to determine the effect of damage on the growth rate of lithospheric drip instabilities. The initial lithospheric viscosity is again set to  $\mu_{\text{max}} = 10^{25}$  Pa s to correspond

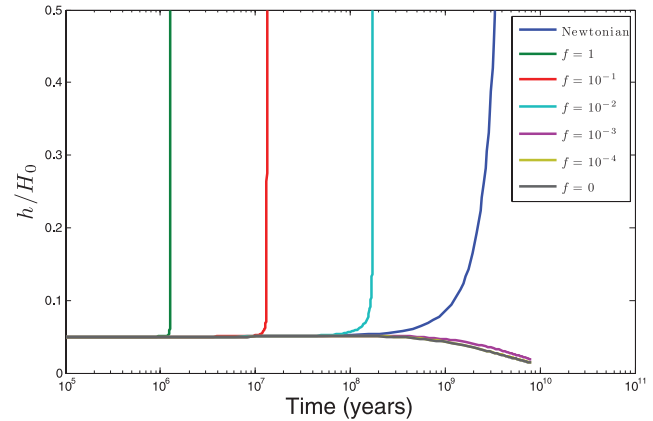


**Figure 2.** Non-dimensional perturbation amplitude as a function of time for the amplitude analysis. When the perturbation amplitude reaches  $0.5H_0$  the characteristic instability time has been reached and a lithospheric drip instability has developed. The blue line is the Newtonian case ( $\tilde{f} = \tilde{k} = 0$ ) which has an instability timescale of  $\tau = 2$  billion years. The other lines include damage with  $\tilde{k} = 6.7$  (corresponding to  $k = 10^{-22} \text{ m}^2 \text{ s}^{-1}$ ) and  $\mathcal{R} = 3.3$ . Here  $H_0 = 320$  km,  $\lambda = 11.4H_0$ ,  $\mu_{\text{max}} = 10^{25}$  Pa s and  $\Delta \rho = 100 \text{ kg m}^{-3}$ . The initial conditions are set to  $h_0 = 0.05H_0$ ,  $\tilde{h}_0 = 0$  and  $\mathcal{A} = 1$ . For this system  $\tilde{f} = 15 \times 10^4 f$ . The lines are labelled for  $f$  so the results are easier to physically interpret. For  $f = 1$ , the timescale is reduced to  $\tau = 1$  million years. Here, only  $f = 1$ ,  $10^{-1}$  and  $10^{-2}$  enhance perturbation growth relative to the Newtonian viscosity. All smaller values of  $f$  collapse down to the  $f = 0$ ,  $\tilde{k} \neq 0$  case (black line).

to the highly viscous lithosphere. We set  $\gamma = 1 \text{ N m}^{-1}$ ,  $A_0 = 10^3 \text{ m}^{-1}$  (corresponding to 1 mm grain size), and use the initial condition  $\mathcal{A} = 1$ . All other parameters are identical to the isoviscous case in Section 3.2.1.

Using the above mentioned parameters, we vary the amount of damage and healing,  $\tilde{f}$  and  $\tilde{k}$ , to determine the sensitivity of perturbation growth to the damage mechanism. We examine three cases  $\tilde{k} = 6.7, 67$  and  $670$ , corresponding to  $k = 10^{-22}, 10^{-21}$  and  $10^{-20} \text{ m}^2 \text{ s}^{-1}$ , which are calculated for olivine using an activation energy of  $200 \text{ kJ mol}^{-1}$  at the temperature of our  $0.5\Delta T + T_s$  isotherm of  $900 \text{ K}$  (Karato 1989). For each case we vary the damage number  $\tilde{f}$  between 0 and  $15 \times 10^4$ , corresponding to  $f$  between 0 and 1 (Fig. 2). We find there is a maximum reduction in the instability timescale when  $\tilde{f} = 15 \times 10^4$ , the largest damage fraction physically possible ( $f = 1$ ). For  $\mathcal{R} = 3.3$ ,  $\tilde{k} = 6.7$  and  $f = 1$ , the characteristic instability timescale is reduced to  $\tau = 1$  million years.

As  $\tilde{f}$  is decreased a critical point is reached where grain growth and thermal diffusion stabilize the perturbation. We define this critical value as  $\tilde{f}_{\text{crit}}$ . When  $\tilde{f} < \tilde{f}_{\text{crit}}$ , grain growth causes the lithosphere to strengthen, slowing the perturbation growth relative to the case with Newtonian viscosity. We find that the critical amount of damage necessary for the formation of lithospheric drip instabilities,  $\tilde{f}_{\text{crit}}$  can be robustly predicted by  $\mathcal{R}$  and  $\tilde{k}$  of the system (Fig. 3). The resulting empirical scaling relationship for  $\tilde{f}_{\text{crit}}$  for the initial conditions  $h_0 = 0.05H_0$ ,  $\tilde{h}_0 = 0$  and  $\mathcal{A} = 1$  and our choice of  $m$  and  $p$  is given as

$$\frac{\tilde{f}_{\text{crit}}}{\tilde{k}} \sim \mathcal{R}^{-1/2}. \quad (20)$$

By including the damage mechanism, the lithosphere can be sufficiently weakened to become entrained in lithospheric drip instabilities. The stress caused by the growing drip mobilizes the highly viscous lithosphere by grain size reduction. However, there is a trade-off between damage and healing such that a minimum amount of damage,  $\tilde{f}_{\text{crit}}$  is required to reduce the characteristic instability timescale. For the realistic rheological parameter values used earlier, the characteristic instability timescale may be reduced to geologically feasible timeframes.

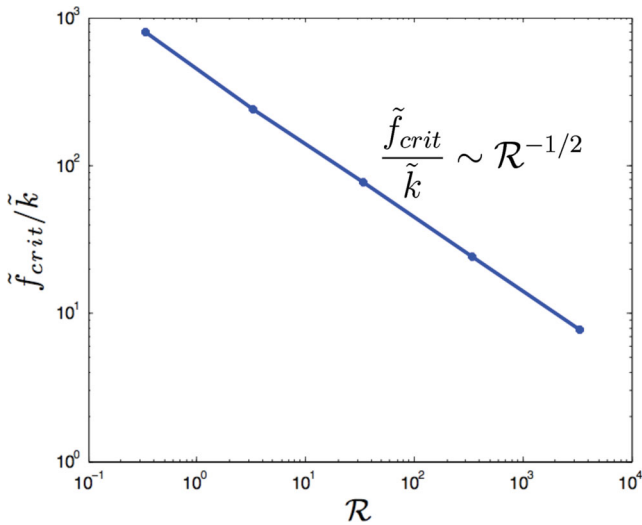


**Figure 3.** Ratio of  $\tilde{f}_{\text{crit}}$  to  $\tilde{k}$  as a function of  $\mathcal{R}$  from the amplitude analysis with initial conditions  $h_0 = 0.05H_0$ ,  $\tilde{h}_0 = 0$  and  $\mathcal{A} = 1$ .  $\tilde{f}_{\text{crit}}/\tilde{k}$  varies as  $\mathcal{R}^{-1/2}$ . Using this relationship we can predict the critical amount of damage necessary for lithospheric drip instabilities to form within geologically reasonable timeframes for a given  $\mathcal{R}$  and  $\tilde{k}$  of the system.

## 4 NUMERICAL SIMULATION OF DRIPS WITH DAMAGE

### 4.1 Model set-up

We employ a 2-D Rayleigh-Bénard convection model to examine the full non-linear development of lithospheric drip instabilities with damage (Landuyt 2009). The model solves Stokes equations for creeping flow with an infinite Prandtl number under the Boussinesq approximation. Unlike previous models that have used simple stress and temperature dependent rheologies, we include damage theory as outlined previously (Bercovici & Ricard 2005; Landuyt *et al.* 2008; Landuyt & Bercovici 2009).

The conservation eqs (1)–(3) are non-dimensionalized according to  $x = Dx'$ ,  $t = (D^2/\kappa)t'$ ,  $\vec{v} = (\kappa/D)\vec{v}'$ ,  $P = (\kappa\mu_{\text{min}}/D^2)$ ,  $\mu = \mu_{\text{min}}\mu'$ ,  $\dot{\epsilon} = (\kappa/D^2)\dot{\epsilon}'$  and  $T = \Delta TT'$ , where  $D$  is the total depth of the lithosphere–mantle system,  $\Delta T$  is the temperature drop across  $D$ ,  $\alpha$  is the thermal expansivity,  $\mu_{\text{min}}$  is the initial viscosity at the bottom of the system and  $\hat{z}$  is the vertical unit vector. The primes are subsequently dropped resulting in (1) being unchanged and (2) and (3) becoming

$$-\nabla P + \nabla \cdot (2\mu\dot{\epsilon}) - Ra_0 T \hat{z} = 0, \quad (21)$$

$$\frac{\partial T}{\partial t} + \vec{v} \cdot \nabla T = \nabla^2 T \quad (22)$$

where the Rayleigh number is given as

$$Ra_0 = \frac{\rho g \Delta T \alpha D^3}{\kappa \mu_{\text{min}}}. \quad (23)$$

These equations are discretized using finite-volumes with a staggered grid and solved via a multigrid method (Landuyt 2009) (Fig. 5a for basic model setup).

The velocity boundary conditions are set to be free slip on the top and bottom and periodic on the sides. The thermal boundary conditions are constant temperature top and bottom boundaries, with bottom heating and no internal heating. We begin with a temperature profile defined by an error function at the top boundary, consistent with that of a half-space cooling model. This temperature profile produces a gravitationally unstable system due to the linear dependence of density on temperature. The viscosity everywhere is grain size and temperature dependent as given by eqs (4) and (5).

We perturb the temperature profile with sinusoids of amplitude  $0.05H_0$  and track the  $0.5\Delta T + T_s$  isotherm which we define as the base of the lithosphere. This isotherm is initially located at depth  $H_0 = 0.15D$ . Due to the finite domain of the model, we use perturbation wavenumbers that correspond to integer multiples of the model width. The simulations are run at  $Ra_0 = 10^5$  which corresponds to  $\alpha\rho\Delta T = \Delta\rho = 100 \text{ kg m}^{-3}$ ,  $D = 2150 \text{ km}$ ,  $\kappa = 10^{-6} \text{ m}^2 \text{ s}^{-1}$  and lower mantle viscosity  $\mu_{\text{min}} = 10^{23} \text{ Pa s}$ . Due to the low Rayleigh number,  $D$  is set to produce a thinner than usual mantle to compensate for the less vigorous than expected convection. Using (4) the Frank-Kamenetskii viscosity ratio  $\bar{\mu}$  is set to  $10^2$ , resulting in an initial lithospheric viscosity ( $\mu_{\text{max}}$ ) equal to  $10^{25} \text{ Pa s}$ . These models have a local Rayleigh number of  $\mathcal{R} = 3.3$  and an aspect ratio of 4. Our resolution is equispaced in the horizontal  $\hat{x}$  and vertical  $\hat{z}$  directions, with  $64 \times 256$  nodes. This analysis is extended to  $Ra_0 = 10^6$  (Appendix B).

To benchmark the numerical model, we compare the Newtonian ( $\tilde{f} = \tilde{k} = 0$ ) perturbation growth rates to those predicted from a linear stability analysis (Appendix A). For  $\bar{\mu} = 10^2$  we find the fastest growing perturbations have wavelengths of  $\lambda = 13.3H_0$  compared

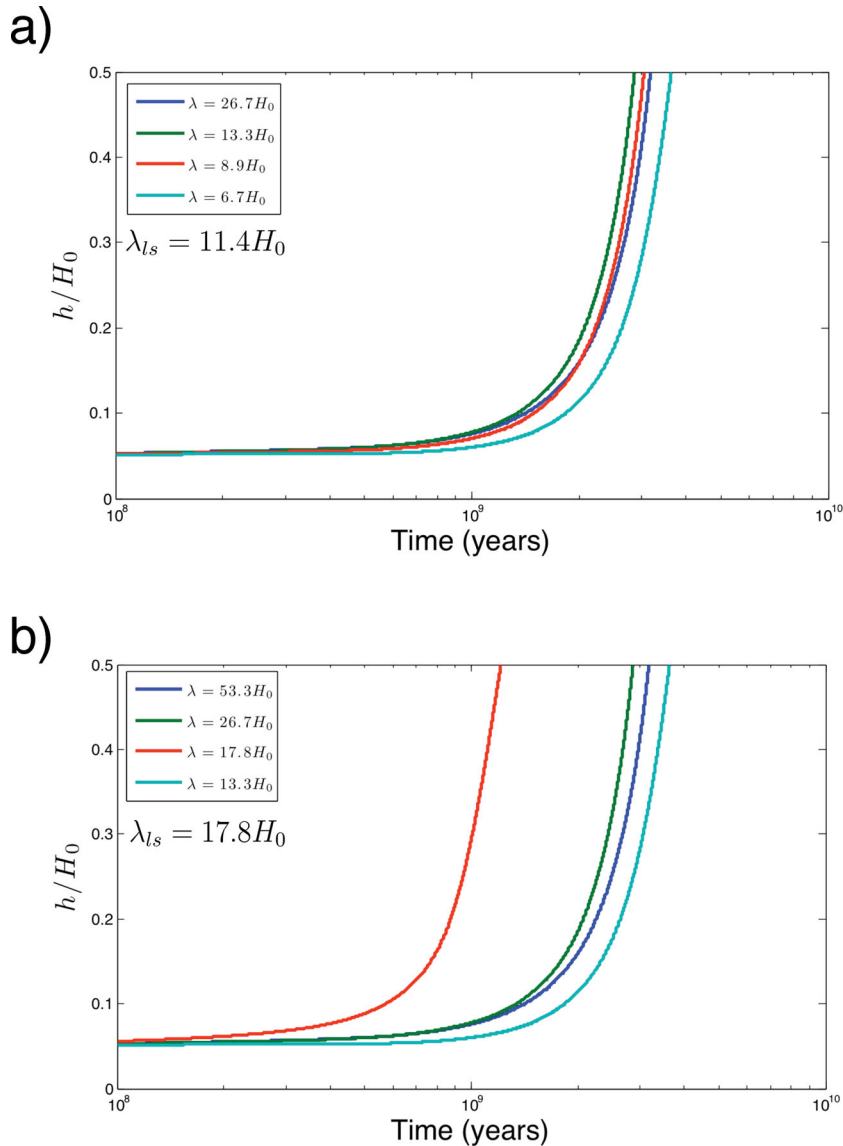


**Figure 4.** Perturbation amplitude from numerical model as a function of time for perturbations of different initial wavelengths. Plots are for Newtonian rheology and viscosity contrasts a)  $\bar{\mu} = 10^2$  and b)  $\bar{\mu} = 10^3$ . The least stable wavelength predicted by the linear stability analysis (Appendix A) is indicated as  $\lambda_{ls}$  on each plot.

to  $\lambda_{ls} = 11.4H_0$  predicted by the linear stability analysis. This is the closest possible values allowed by the finite domain of the numerical model. We also find that the growth rates for each mode agree well initially between the linear stability analysis and the numerical model. The growth of the perturbation over time is found by tracking the evolution of the temperature field, where we track the base of the lithosphere as the  $0.5\Delta T + T_s$  isotherm (Fig. 5). In the numerical model, the formation of a lithospheric drip instability using a Newtonian lithospheric viscosity of  $\mu_{\max} = 10^{25}$  Pa s requires  $\sim 2$  billion years, consistent with the linear stability analysis.

## 4.2 Damage results

We now include the grain size dependence in the numerical model by setting  $\tilde{f} \neq 0$  and  $\tilde{k} \neq 0$ . As in the previous sections, we set  $\bar{\mu} = 10^2$  with  $Ra_0 = 10^5$  to produce an initial lithospheric viscosity of  $10^{25}$  Pa s. We use initial perturbations corresponding to the least

stable mode, as described earlier. Similar to the amplitude analysis, we set  $m = 2$  and  $p = 3$  to match experiments. We consider three values of  $\tilde{k}$ ,  $\tilde{k} = 3.1, 31$  and  $310$ , corresponding to the same  $k$  values in the amplitude analysis;  $k = 10^{-22}, 10^{-21}$  and  $10^{-20} \text{ m}^2 \text{ s}^{-1}$ , we vary  $f$  between 0 and 1, which now corresponds to  $\tilde{f}$  between 0 and  $32 \times 10^4$ . We set  $\gamma = 1 \text{ N m}^{-1}$ , use the initial condition  $\mathcal{A} = 1$  and all other values are as in the Newtonian viscosity case mentioned above.

We use the amplitude analysis to predict  $\tilde{f}_{\text{crit}}$  for the  $\mathcal{R}$  and  $\tilde{k}$  values of each numerical case (indicated on Fig. 6). Using the numerical model, we find that in all cases perturbation growth is only enhanced for  $\tilde{f} > \tilde{f}_{\text{crit}}$ , where the instability timescale can be reduced to  $\tau = 10$  million years (Fig. 6a). For  $\tilde{f} > \tilde{f}_{\text{crit}}$  the amount of damage is sufficient to localize deformation through grain size reduction. The corresponding fineness fields show a significant grain size reduction localized where the stresses from the growing perturbations are high (Figs 7a–c), which in turn creates localized weakening in the highly viscous lithosphere (Figs 7d–f). Relative to

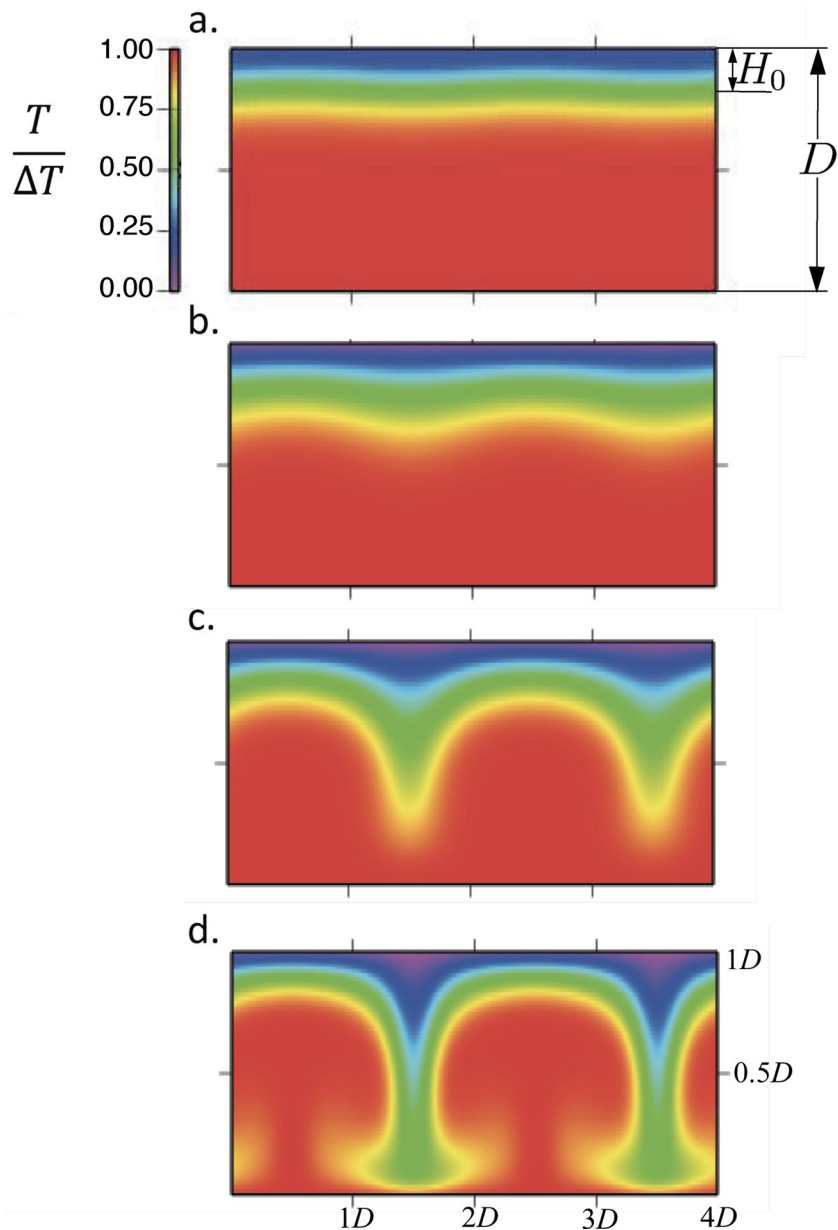


**Figure 5.** Time progression of the thermal field for the numerical model with a Newtonian viscosity ( $\tilde{f} = \tilde{k} = 0$ ),  $\bar{\mu} = 10^2$ ,  $Ra_0 = 10^5$  and  $\lambda = 13.3H_0$ . a, b, c and d correspond to 0, 15, 30 and 45 billion years. The perturbation growth is given by the time evolution of the  $0.5\Delta T + T_s$  isotherm, initially located at  $H_0 = 0.15D$  (a), where  $\Delta T$  is the potential temperature drop over the depth  $D$  of the lithosphere–mantle system. A width of  $4D$  is used for  $\bar{\mu} = 10^2$ ,  $Ra_0 = 10^5$  runs and in Appendix B a width of  $8D$  is used for the  $\bar{\mu} = 10^3$  and  $Ra_0 = 10^6$  runs. All cases are run with a depth  $D$  and an equispaced grid of  $64 \times 256$  or  $64 \times 512$  nodes.

the Newtonian case, this localized weakening effectively mobilizes the highly viscous upper lithosphere (Figs 7h–i). The flow patterns indicate substantially more movement of the highly viscous lithosphere when  $f > f_{\text{crit}}$  (Fig. 8a), with the higher rms velocity in the upper viscous lithosphere when significant damage is present than for only a Newtonian viscosity (Fig. 8b).

For cases with  $\tilde{f} < \tilde{f}_{\text{crit}}$  the perturbation decays. The corresponding fineness fields for these cases reveal a gradual, overall grain growth and associated viscosity increase. The increase in viscosity reduces the growth rate of the perturbation enough for thermal diffusion to dominate, causing the perturbation to decay. This suppresses the development of drip instabilities relative to the cases with Newtonian viscosity.

## 5 DISCUSSION

We use our model to explain the observed formation of large volume drip instabilities in convergent and extensional tectonic settings (Houseman *et al.* 1981; England & Houseman 1988, 1989; Ghosh *et al.* 2006a,b; Garzzone *et al.* 2006; Rowley & Garzzone 2007; Hoke & Garzzone 2008; Garzzone *et al.* 2008; Humphreys & Clayton 1990; Jones *et al.* 1994; Saleeby & Foster 2004; Boyd *et al.* 2004; Zandt *et al.* 2004; Yang & Forsyth 2006; Ducea & Saleeby 1996; Saleeby *et al.* 2003; West *et al.* 2009). The added damage physics (Bercovici & Ricard 2005; Landuyt *et al.* 2008; Landuyt & Bercovici 2009) results in localized weakening and mobilization of the highly viscous lithosphere suggesting lithospheric drip

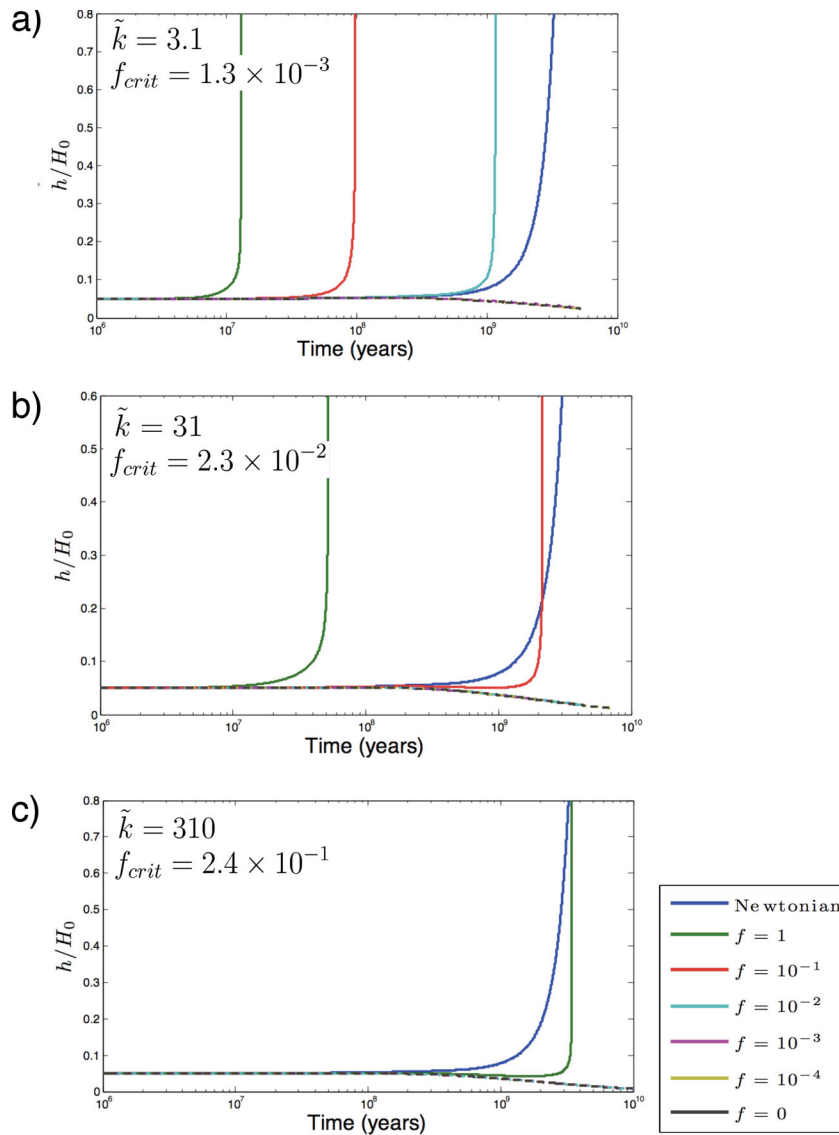


**Figure 6.** Perturbation amplitude as a function of time for the numerical model with  $\bar{\mu} = 10^2$ ,  $\lambda = 13.3H_0$ ,  $H_0 = 0.15D$ ,  $D = 2150$  km and  $Ra_0 = 10^5$ . When the perturbation amplitude reaches  $0.5H_0$  a lithospheric drip instability has developed. Healing rate  $\tilde{k}$  is constant as shown on each plot while  $f$  is varied between 0 and 1. In all cases above  $\mathcal{R} = 3.3$ . The amplitude analysis is used to calculate  $\tilde{f}_{crit}$ , which is converted to  $f_{crit}$  and shown on each plot. Only for cases where  $f > f_{crit}$  (solid lines) is perturbation growth enhanced relative to the Newtonian viscosity ( $f = \tilde{k} = 0$ ) shown in blue. Cases with  $f < f_{crit}$  are shown in dashed lines. All cases with  $f < f_{crit}$  collapse down to the  $f = 0$ ,  $\tilde{k} \neq 0$  case (black line).

instabilities can form from small perturbations, as a natural consequence of the thermal and rheological properties of the Earth, independent of tectonic setting. Our model does not include any external forcing (e.g. convergence), and the drips arise from only small perturbations to the thermal structure of the system. Such small perturbations could be present in convergent, extensional, or non-tectonically active zones, greatly expanding possible locations for large volume drips. The relatively short timescales of large volume drip formation and the expanded tectonic settings suggest a new mechanism for large-volume lithospheric recycling and has implications for the overall stability and longevity of the lithosphere.

Although relatively small perturbations may lead to large volume drip formation, these perturbations do not always form into large volume drip instabilities. Instead, we find that a critical amount of damage  $\tilde{f}_{crit}$  is necessary for a drip instability to develop.  $\tilde{f}_{crit}$  is

largely dependent on quantities from mineral physics experiments, specifically the value of  $k$  and how  $k$  varies with temperature. In this study, we chose  $k$  based on the (Karato 1989) experiments for olivine with activation energy of  $200 \text{ kJ mol}^{-1}$ , which can be considered a lower limit compared to more recent values (Evans *et al.* 2001). If higher activation energies are used, grain growth is slowed by several orders of magnitude, further enhancing drip formation. Better mineral physics constraints on  $f$  and  $k$ , through improved understanding of grain size evolution and grain size dependent rheologies, will allow for the prediction of lithospheric drip formation in specific geographic regions.

Drip formation is also somewhat sensitive to the initial perturbation amplitude. We find there exists a minimum initial perturbation amplitude,  $h_0 = 0.05H_0$ , below which perturbations decay due to thermal diffusion. For perturbations larger than  $h_0 = 0.05H_0$ , instability growth is possible when sufficient amounts of damage

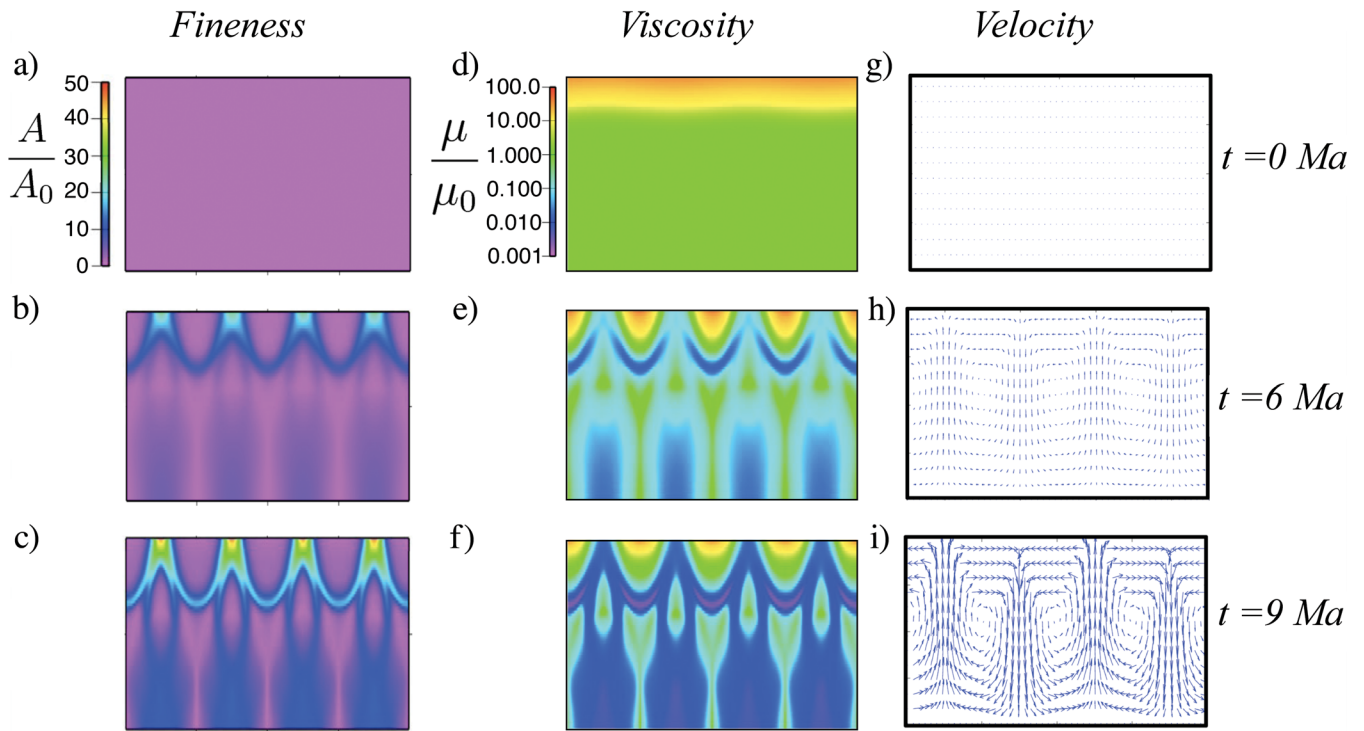


**Figure 7.** Time progression of the fineness (a–c), viscosity (d–f) and velocity (g–i) fields from the numerical model with  $f = 1$ , such that  $\tilde{f} > \tilde{f}_{\text{crit}}$ . Here  $\bar{\mu} = 10^2$ ,  $Ra_0 = 10^5$ ,  $\lambda = 13.3H_0$  and  $k = 10^{-22} \text{ m}^2 \text{ s}^{-1}$ , corresponding to  $\mathcal{R} = 3.3$  and  $\tilde{k} = 3.1$ . Because  $\tilde{f} > \tilde{f}_{\text{crit}}$ , grain size is locally reduced in regions of high stress around the perturbation. The reduced grain size weakens the material, resulting in an enhanced perturbation growth rate. Plots progress forward in time down the page with times 0, 6 and 9 million years.

exist in the system. To generalize our analysis we have used the smallest initial perturbation amplitude that leads to damage enhanced lithospheric drip growth. Furthermore, larger initial perturbations also have larger growth rates, suggesting instabilities will develop most rapidly in regions containing large perturbations, such as convergent tectonic settings. Therefore, although we suggest large-volume lithospheric instabilities may arise independently of tectonic settings, when  $\tilde{f} > \tilde{f}_{\text{crit}}$ , our results do not exclude instability-enhancing tectonic forcing, including convergence induced thickening or dense magmatic emplacement.

In areas of convergence the lithosphere has been thickened, increasing  $H_0$ , which results in larger  $\mathcal{R}$  values. Similarly, in areas of dense magma emplacement the density contrast,  $\Delta\rho$ , is increased resulting in an increase in  $\mathcal{R}$ . Our amplitude analysis indicates that the minimum amount of damage required for a drip instability to develop,  $\tilde{f}_{\text{crit}}$ , is related to the non-dimensional healing rate  $\tilde{k}$  and local Rayleigh number  $\mathcal{R}$  by (20). In both of these settings, the effect of increasing  $\mathcal{R}$  will result in decreasing  $\tilde{f}_{\text{crit}}$ . Lower  $\tilde{f}_{\text{crit}}$  means that in addition to overall faster rates of perturbation growth in these settings, a smaller amount of damage is required for a drip instability to develop. Therefore, although our theory predicts that drip instabilities can develop independent of tectonic forcing, regions of convergent thickening and dense magmatic emplacement may be more prone to developing large volume drip instabilities. The lithospheric thickening and dense magmatic emplacement present in these tectonic settings all lower  $\tilde{f}_{\text{crit}}$  such that less damage induced weakening is required to reach the criteria  $\tilde{f} > \tilde{f}_{\text{crit}}$ . Reduced  $\tilde{f}_{\text{crit}}$  in these areas may explain why the majority or large volume drips have been found in tectonic settings with convergent thickening and dense magmatic emplacement.

## 6 CONCLUSIONS

Large volume lithospheric drip instabilities are second-scale convective features that have been found under regions of continental lithosphere. Previous models suggested that the formation of these instabilities required forced thickening of the mobile base of the lithosphere or magmatic emplacement of dense lithosphere. Here, we use damage physics appropriate for plate generation on Earth to re-examine the formation of these instabilities in the absence of such tectonic forcing. By partitioning a fraction of deformational work into surface energy to reduce grain size, the damage mechanism creates localized weakening that mobilizes the highly viscous lithosphere, which facilitates entrainment of upper lithosphere in the growing drip instability, increasing both the volume and the growth rate of the drip instability.

Our system can be parameterized by a critical damage value  $\tilde{f}_{\text{crit}}$ , which is easily estimated by the amplitude analysis using  $\mathcal{R}$  and  $\tilde{k}$ , and accurately predicts the behaviour of the numerical model. For  $\tilde{f} < \tilde{f}_{\text{crit}}$  thermal diffusion and grain growth dominate, and perturbations to the base of the lithosphere decay due to diffusive smoothing, thus perturbation growth is suppressed relative to the case of Newtonian viscosity. For  $\tilde{f} > \tilde{f}_{\text{crit}}$ , the localized weakening mobilizes the highly viscous lithosphere, allowing it to become entrained in the growing drip at a rate faster than with a Newtonian viscosity. The inclusion of the highly viscous lithosphere increases the volume of the drip instability. As the drip continues to grow, the increase in negative buoyancy, combined with damage induced weakening, accelerates the growth of the drip instability such that drip formation occurs within geologically feasible timeframes. The numerical results indicate that the characteristic instability timescale may be reduced from  $\sim 2$  billion years, as with a Newtonian

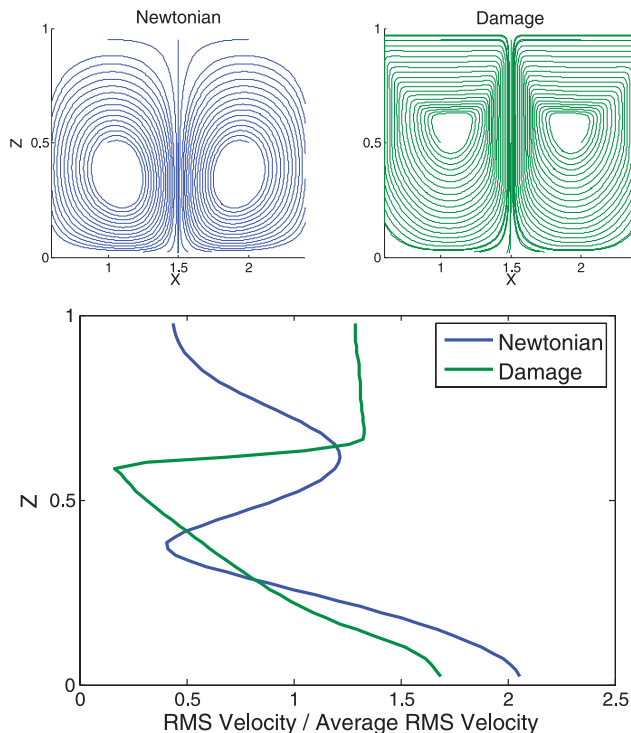


**Figure 8.** Effects of damage on the streamlines and RMS velocity in the highly viscous upper lithosphere. Newtonian viscosity ( $\tilde{f} = \tilde{k} = 0$ ) is shown in blue, while damage ( $\tilde{f} > f_{\text{crit}}, \tilde{k} \neq 0$ ) is shown in green. Damage is plotted for  $\tilde{f} = 32 \times 10^4$ ,  $\tilde{k} = 3.1$ , corresponding to  $f = 1$ ,  $k = 10^{-22} \text{ m}^2 \text{ s}^{-1}$ . In both cases  $\bar{\mu} = 10^2$ ,  $\lambda = 13.3H_0$ ,  $H_0 = 0.15D$ ,  $D = 2150 \text{ km}$ ,  $Ra_0 = 10^5$  and  $\mathcal{R} = 3.3$ . All plots centred around a downwelling drip and are shown for perturbation height of  $0.1H_0$ , which occurs at 1 billion years for the Newtonian case and 10 million years for the damage case. The two stream function plots have the same contour interval and the RMS velocities are depth averaged and normalized by their respective average non-dimensional RMS velocity, three for the Newtonian viscosity and 6500 for the case with damage.

viscosity, to  $\sim 10$  million years for plausible damage parameters. Our results suggest that when localized weakening is included, large volume lithospheric drip instabilities may form independent of external tectonic forcing.

## REFERENCES

Armijo, R., Tapponnier, P., Mercier, J. & Han, T., 1986. Quaternary extension in southern Tibet, *J. geophys. Res.*, **91**, 13 803–13 872.

Austin, N. & Evans, B., 2007. Paleowattmeters: a scaling relation for dynamically recrystallized grain size, *Geology*, **35**, 343–346.

Bercovici, D., 2003. The Generation of plate tectonics from mantle convection, *Earth planet. Sci. Lett.*, **205**, 107–121.

Bercovici, D. & Ricard, Y., 2003. Energetics of a two-phase model of lithospheric damage, shear localization and plate-boundary formation, *Geophys. J. Int.*, **152**, 581–596.

Bercovici, D. & Ricard, Y., 2005. Tectonic plate generation and two-phase damage: void growth versus grain size reduction, *J. geophys. Res.*, **110**, 1–18.

Bercovici, D., Ricard, Y. & Richards, M., 2000. The relation between mantle dynamics and plate tectonics: a primer, in *History and Dynamics of Global Plate Motions*, Geophys. Monogr. Ser. Vol. 121, pp. 5–46, American Geophysical Union, Washington, DC.

Bercovici, D., Ricard, Y. & Schubert, G., 2001a. A two-phase model of compaction and damage, 1. General theory, *J. geophys. Res.*, **106**(B5), 8887–8906.

Bercovici, D., Ricard, Y. & Schubert, G., 2001b. A two-phase model of compaction and damage, 3. Applications to shear localization and plate boundary formation, *J. geophys. Res.*, **106**(B5) 8925–8940.

Boyd, O., Jones, C. & Sheehan, A., 2004. Foundering lithosphere imaged beneath the Southern Sierra Nevada, California, USA, *Science*, **305**, 660–662.

Buck, W.R. & Parmentier, E., 1986. Convection beneath young oceanic lithosphere: implications for thermal structure and gravity, *J. geophys. Res.*, **91**, 1961–1974.

Chang, C. et al., 1986. Preliminary conclusions of the Royal Society and Academia Sinica 1985 geotraverse of Tibet, *Nature*, **323**, 510–507.

Chen, W.-P. & Molnar, P., 1983. Focal depths of intracontinental and intraplate earthquakes and their implications for the thermal and mechanical properties of the lithosphere, *J. geophys. Res.*, **88**, 4183–4214.

Conrad, C., 2000. Convective instability of thickening mantle lithosphere, *Geophys. J. Int.*, **143**, 52–70.

Conrad, C. & Molnar, P., 1997. The growth of Rayleigh-Taylor-type instabilities in the lithosphere for various rheological and density structures, *Geophys. J. Int.*, **129**, 95–112.

Ducea, M. & Saleeby, J., 1996. Buoyancy sources for a large, unrooted mountain range, the Sierra Nevada, California: evidence from xenolith thermobarometry, *J. geophys. Res.*, **101**, 8229–8244.

Dumoulin, C., Doin, M. & Fleitout, L., 2001. Numerical simulations of the cooling of an oceanic lithosphere above a convective mantle, *Phys. Earth planet. Inter.*, **125**, 45–64.

Dumoulin, C., Doin, M., Arcay, D. & Fleitout, L., 2005. Onset of small-scale instabilities at the base of the lithosphere: scaling laws and role of pre-existing lithospheric structures, *Geophys. J. Int.*, **160**, 345–357.

Elkins-Tanton, L. & Hager, B., 2000. Melt intrusion as a trigger for lithospheric foundering and the eruption of the Siberian flood basalts, *Geophys. Res. Lett.*, **27**, 3937–3940.

England, P. & Houseman, G., 1988. The mechanics of the Tibetan Plateau, *Phil. Trans. R. Soc. Lond. A*, **326**, 301–320.

England, P. & Houseman, G., 1989. Extension during continental convergence with application to the Tibetan Plateau, *J. geophys. Res.*, **94**, 17 561–17 579.

Evans, B., Renner, J. & Hirth, G., 2001. A few remarks on the kinetics of static grain growth in rocks, *Int. J. Earth Sci.*, **90**, 88–103.

Garzone, C., Molnar, P., Libarkin, J. & MacFadden, B., 2006. Rapid late Miocene rise of the Bolivian Altiplano: evidence for removal of mantle lithosphere, *Earth planet. Sci. Lett.*, **241**, 543–556.

Garzone, C., Hoke, G., Libarkin, J., Withers, S., MacFadden, B., Eiler, J., Ghosh, P. & Mulch, A., 2008. Rise of the Andes, *Science*, **320**, 1304–1307.

Ghosh, P., Adkins, J., Affek, H., Balta, B., Guo, W., Schauble, E., Schrag, D. & Eiler, J., 2006a.  $^{13}\text{C}$ - $^{18}\text{O}$  bonds in carbonate minerals: a new kind of paleothermometer, *Geochim. Cosmochim. Acta*, **70**, 1439–1456.

Ghosh, P., Garzone, C. & Eiler, J., 2006b. Rapid uplift of Altiplano revealed through  $^{13}\text{C}$ - $^{18}\text{O}$  bonds in paleosol carbonates, *Science*, **311**, 511–515.

Hoke, G. & Garzone, C., 2008. Paleosurfaces, paleoelevation, and the mechanisms for the late Miocene topographic development of the Altiplano plateau, *Earth planet. Sci. Lett.*, **271**, 192–201.

Houseman, G. & McKenzie, D., 1982. Numerical experiments on the onset of convective instability in the Earth's mantle, *Geophys. J. R. astr. Soc.*, **68**, 133–164.

Houseman, G. & Molnar, P., 1997. Gravitational (Rayleigh-Taylor) instability of a layer with a non-linear viscosity and convective thinning of continental lithosphere, *Geophys. J. Int.*, **128**, 125–150.

Houseman, G. & Molnar, P., 2001. Mechanisms of lithospheric rejuvenation associated with continental orogeny, *Geol. Soc. Lond., Spec. Publ.*, **184**, 13–38.

Houseman, G., McKenzie, D. & Molnar, P., 1981. Convective instability of a thickened boundary layer and its relevance for the thermal evolution of continental convergent belts, *J. geophys. Res.*, **86**, 6115–6132.

Huang, J., Zhong, S. & van Hunen, J., 2003. Controls on sublithospheric small-scale convection, *J. geophys. Res.*, **108**, doi:10.1029/2003JB002456.

Humphreys, E. & Clayton, R., 1990. Tomographic Image of the Southern California Mantle, *J. geophys. Res.*, **95**, 19725–19746.

- Jones, C., Kanamori, H. & Roecker, S., 1994. Missing roots and mantle “drips”: regional  $P_n$  and teleseismic arrival times in the southern Sierra Nevada and vicinity, California, *J. geophys. Res.*, **99**, 4567–4601.
- Jull, M. & Kelemen, P., 2001. On the conditions of lower crustal convective instability, *J. geophys. Res.*, **106**, 6423–6446.
- Karato, S., 1989. Grain growth kinetics in olivine aggregates, *Tectonophysics*, **168**, 255–273.
- Korenaga, J. & Jordan, T., 2003. Physics of multiscale convection in Earth’s mantle: onset of sublithospheric convection, *J. geophys. Res.*, **108**, doi:10.1029/2002JB001760.
- Landuyt, W., 2009. The generation of plate tectonics on a planet, *PhD thesis*, Yale University, New Haven, CT.
- Landuyt, W. & Bercovici, D., 2009. Formation and structure of lithospheric shear zones with damage, *Phys. Earth planet. Inter.*, **175**, 115–126.
- Landuyt, W., Bercovici, D. & Ricard, Y., 2008. Plate generation and two-phase damage theory in a model of mantle convection, *Geophys. J. Int.*, **174**, 1065–1080.
- Lev, E. & Hager, B., 2008. Rayleigh-Taylor instabilities with anisotropic lithospheric viscosity, *Geophys. J. Int.*, **173**, 806–814.
- Lin, J. & Watts, D., 1988. Paleomagnetic constraints on Himalaya-Tibetan tectonic evolution, *Phil. Trans. R. Soc. Lond., A*, **326**, 177–188.
- McKenzie, D. & Sclater, J., 1971. The evolution of the Indian Ocean since the Late Cretaceous, *Geophys. J. Int.*, **24**, 437–528.
- Molnar, P. & Tapponnier, P., 1975. Cenozoic tectonics of Asia: effects of a continental collision, *Science*, **189**, 419–426.
- Molnar, P., Tapponnier, P. & Chen, W.-P., 1981. Extensional tectonics in central and eastern Asia: a brief summary, *Phil. Trans. R. Soc. Lond. A*, **300**, 403–406.
- Molnar, P., England, P. & Martinod, J., 1993. Mantle dynamics, uplift of the Tibetan Plateau, and the Indian Monsoon, *Rev. Geophys.*, **31**, 357–396.
- Molnar, P., Houseman, G. & Conrad, C., 1998. Rayleigh-Taylor instabilities and convective thinning of mechanically thickened lithosphere: effects of non-linear viscosity decreasing exponentially with depth and of horizontal shortening of the layer, *Geophys. J. Int.*, **133**, 568–584.
- Murphy, M., Saylor, J. & Ding, L., 2009. Late Miocene topographic inversion in southwest Tibet based on paleoelevation reconstructions and structural history, *Earth planet. Sci. Lett.*, **282**, 1–9.
- Neil, E. & Houseman, G., 1999. Rayleigh-Taylor instability of the upper mantle and its role in intraplate orogeny, *Geophys. J. Int.*, **138**, 89–107.
- Patriat, P. & Achache, J., 1984. India-Eurasia collision chronology has implications for crustal shortening and driving mechanism of plates, *Nature*, **311**, 615–621.
- Platt, J. & England, P., 1993. Convective removal of lithosphere beneath mountain belts: thermal and mechanical consequences, *Am. J. Sci.*, **293**, 307–336.
- Rowley, D. & Garzzone, C., 2007. Stable Isotope-Based Paleothermometry, *Annu. Rev. Earth planet. Sci.*, **35**, 463–508.
- Rozel, A., Ricard, Y. & Bercovici, D., 2010. A thermodynamically self-consistent damage equation for grain size evolution during dynamic recrystallization, *Geophys. J. Int.*, **184**, doi: 10.1111/j.1365-246X.2010.04875.x.
- Saleeby, J. & Foster, Z., 2004. Topographic response to the mantle lithosphere removal in the southern Sierra Nevada region, California, *Geology*, **32**, 245–248.
- Saleeby, J., Ducea, M. & Clemens-Knott, D., 2003. Production and loss of high-density batholithic root, southern Sierra Nevada, California, *Tectonics*, **22**, C001374, doi:10.1029/2002TC001374.
- Tackley, P., 2000. The quest for self-consistent generation of plate tectonics in mantle convection models, in *History and Dynamics of Global Plate Motions*, Geophys. Monogr. Ser. Vol. 121, pp. 47–72, American Geophysical Union, Washington, DC.
- Tapponnier, P. et al., 1981. The Tibetan side of the India-Eurasia collision, *Nature*, **294**, 405–410.
- West, J., Fouch, M., Roth, J. & Elkins-Tanton, L., 2009. Vertical mantle flow associated with a lithospheric drip beneath the Great Basin, *Nat. Geosci.*, **2**, 439–444.
- Yang, Y. & Forsyth, D., 2006. Rayleigh wave phase velocities, small-scale convection, and azimuthal anisotropy beneath southern California, *J. geophys. Res.*, **111**, B07306, doi:10.1029/2005JB004180.
- Yuen, D. & Fleitout, L., 1985. Thinning of the lithosphere by small-scale convection destabilization, *Nature*, **313**, 125–128.
- Zandt, G., Gilbert, H., Owens, T., Ducea, M., Saleeby, J. & Jones, C., 2004. Active foundering of a continental arc root beneath the southern Sierra Nevada in California, *Nature*, **431**, 41–46.

## APPENDIX A: LINEAR STABILITY

We perform a linear stability analysis to determine the least stable mode for perturbations to a system with a dense lithospheric layer over-lying a less dense mantle half-space. The least stable mode corresponds to the perturbation wavelength with the fastest initial growth rate and is therefore most likely to control the formation of a lithospheric drip instability. Both of these regions have constant, Newtonian viscosities, defined by the viscosity contrast  $\bar{\mu} = \mu_{\max}/\mu_{\min}$ , where we set  $\mu_l = \mu_{\max}$  and  $\mu_m = \mu_{\min}$ , and the subscripts  $l$  and  $m$  refer to the lithosphere and mantle. The density difference between the layer and the half space is  $\Delta\rho = \rho_l - \rho_m$ . Here we approximate a lithospheric drip instability as a Rayleigh-Taylor instability by assuming the perturbation growth rates are much faster than thermal diffusion.

The location of the interface between the layer and the half space is perturbed by  $h$  (a white noise wavenumber power spectrum). The growth rate of this perturbation is calculated as a function of the perturbation wavenumber,  $\nu$ , and  $\bar{\mu}$ . We begin our analysis by determining the velocity field in both the lithosphere and the mantle. Eqs (1) and (2) for an incompressible, isoviscous fluid become

$$\nabla \cdot \vec{v}_i = 0, \quad i = l, m \quad (\text{A1})$$

$$-\nabla p_i + \mu_i \nabla^2 \vec{v}_i + \rho_i g = 0, \quad i = l, m. \quad (\text{A2})$$

Eq. (A1) is used to write the 2-D velocity fields in terms of the streamfunction,  $\psi$ , as

$$v_i = \nabla \times \psi_i \hat{y}, \quad i = l, m, \quad (\text{A3})$$

where  $\hat{y} = \hat{z} \times \hat{x}$  and  $\hat{x}$  and  $\hat{z}$  are unit vectors in the horizontal and vertical directions. For an isoviscous lithosphere and mantle, inserting (A3) into (A2) we obtain the differential equation for  $\psi$  as

$$\nabla^4 \psi_i = 0, \quad i = l, m. \quad (\text{A4})$$

Assuming our system is periodic in the horizontal direction, we write the solutions in terms of a Fourier series, solving for the growth rate as a function of  $\nu$ . The general form for the solution to the biharmonic equation (A4) in terms of  $\nu$  is given by

$$\psi = \sum_{\nu=-\infty}^{\infty} ((A_\nu + B_\nu \nu z) e^{\nu z} + (C_\nu + D_\nu \nu z) e^{-\nu z}) e^{i\nu x}, \quad (\text{A5})$$

where the subscript  $\nu$  indicates the function is in Fourier space.

We examine a lithosphere–mantle system with a free-slip top boundary such that there is zero vertical velocity ( $\vec{v} \cdot \hat{n} = 0$ ) and no shear stress ( $\hat{n} \times \underline{\sigma}_{\text{tot}} \cdot \hat{n} = 0$ ), where  $\hat{n}$  is the unit normal vector defining the top boundary and  $\underline{\sigma}_{\text{tot}}$  is the total stress tensor. At the lithosphere–mantle interface ( $z = h$ ) velocity and stress are continuous, so the jump in shear velocity, normal velocity, shear stress and normal stress must be zero across the interface. This equates to  $[\vec{v} \times \hat{n}]'_m = 0$ ,  $[\vec{v} \cdot \hat{n}]'_m = 0$ ,  $[\hat{n} \times \underline{\sigma}_{\text{tot}} \cdot \hat{n}]'_m = 0$  and  $[\hat{n} \cdot \underline{\sigma}_{\text{tot}} \cdot \hat{n}]'_m = 0$ , where here  $\hat{n}$  defines the lithosphere–mantle interface. The flow must also be finite as  $z \rightarrow -\infty$ .

Using the boundary conditions above to solve (A4) and linearizing around  $z = 0$  (i.e.  $||h|| < 1$ ), we calculate the streamfunction in both the lithosphere and the mantle. We then calculate the perturbation growth rate using the kinematic constraint that the normal component of the velocity evaluated at the lithosphere–mantle interface ( $z = h$ ) equals the growth rate  $S$  of the perturbation to that interface as a function of perturbation wavenumber  $\nu$  and  $\bar{\mu}$ ,

$$S = \frac{1}{h\nu} \text{iv}\psi_v|_{z=h}. \quad (\text{A6})$$

For a given  $\mu_m$ , as  $\bar{\mu}$  increases the maximum growth rate decreases following the function  $S_{\text{max}} = 0.23\bar{\mu}^{-1}$ . For a constant  $\mu_l$ ,  $S_{\text{max}}$  becomes invariant to changes in  $\bar{\mu}$ , and is  $2.3 \times 10^{-16} \text{ s}^{-1}$  for  $\mu_l = 10^{25} \text{ Pa s}$ . This indicates the initial growth rate of the lithospheric drip instabilities is determined solely by the viscous resistance of the lithosphere  $\mu_l$ , the region of the system with the highest viscosity. The wavelengths of the least stable modes,  $\lambda_{ls}$ , for the viscosity contrasts used in this study  $\bar{\mu} = 10^2$  and  $10^3$  are 10–20 lithospheric thicknesses,  $H_0$ , a result consistent with a free surface top boundary condition under convergence (Conrad & Molnar 1997; Neil & Houseman 1999).

To benchmark the numerical model, we compare the Newtonian ( $\tilde{f} = \tilde{k} = 0$ ) perturbation growth rates to those predicted from a linear stability analysis. For  $\bar{\mu} = 10^2$  and  $10^3$  we find the fastest growing perturbations have wavelengths that are the closest possible values to those predicted by the linear stability analysis allowed by the finite domain of the numerical model (Fig. 4). We therefore use  $\lambda = 13.3H_0$  and  $\lambda = 17.8H_0$  for our numerical models with  $\bar{\mu} = 10^2$  and  $10^3$ , respectively.

## APPENDIX B: EXTENSION TO HIGHER RAYLEIGH NUMBER

We run our numerical model for  $Ra_0 = 10^6$ , which corresponds to a lower mantle viscosity of  $\mu_{\text{min}} = 10^{22} \text{ Pa s}$  since  $D$  and  $\Delta T$  are kept the same as the  $Ra_0 = 10^5$  case. Using (4) the Frank-Kamenetskii viscosity ratio  $\bar{\mu}$  is set to  $10^3$ , resulting in an initial lithospheric viscosity ( $\mu_{\text{max}}$ ) equal to  $10^{25} \text{ Pa s}$ . Similarly to the  $Ra_0 = 10^5$  cases, the local Rayleigh number is  $\mathcal{R} = 3.3$ . For  $\mu = 10^3$  we find that the fastest growing perturbation has a wavelength of  $\lambda = 17.8H_0$  (Fig. 4b), which matches that predicted by the linear stability analysis (Appendix A). These  $\bar{\mu} = 10^3$  runs have an aspect ratio of 8 to accommodate their longer least stable wavelength. The resolution is equispaced in the horizontal  $\hat{x}$  and vertical  $\hat{z}$  directions, with  $64 \times 512$  nodes.

We begin with the case of a Newtonian viscosity ( $\tilde{f} = \tilde{k} = 0$ ) and find that the formation of lithospheric drip instabilities requires  $\tau = 1$  billion years. We then consider the same three cases for  $\tilde{k}$  as with the  $Ra_0 = 10^5$  runs,  $\tilde{k} = 3.1, 31$  and  $310$ , which correspond to  $k = 10^{-22}, 10^{-21}$  and  $10^{-20} \text{ m}^2 \text{ s}^{-1}$ . We vary  $f$  between 0 and 1 ( $\tilde{f}$  between 0 and  $32 \times 10^4$ ). All other variables are kept the same as the  $Ra_0 = 10^5$  case. We use the amplitude analysis to predict  $\tilde{f}_{\text{crit}}$  for the  $\mathcal{R}$  and  $\tilde{k}$  values of each numerical case (indicated on Fig. B1). Similarly to the  $Ra_0 = 10^5$  cases, we find that perturbation growth is only enhanced for  $\tilde{f} > \tilde{f}_{\text{crit}}$  (Fig. B1). The characteristic instability timescale is reduced to  $\tau = 4$  million years (Fig. B1a). Furthermore, all of these cases follow the scaling relation give in (20), indicating that the amplitude analysis can be extended to predict the behaviour of systems with higher convective Rayleigh numbers, closer to those expected on Earth.

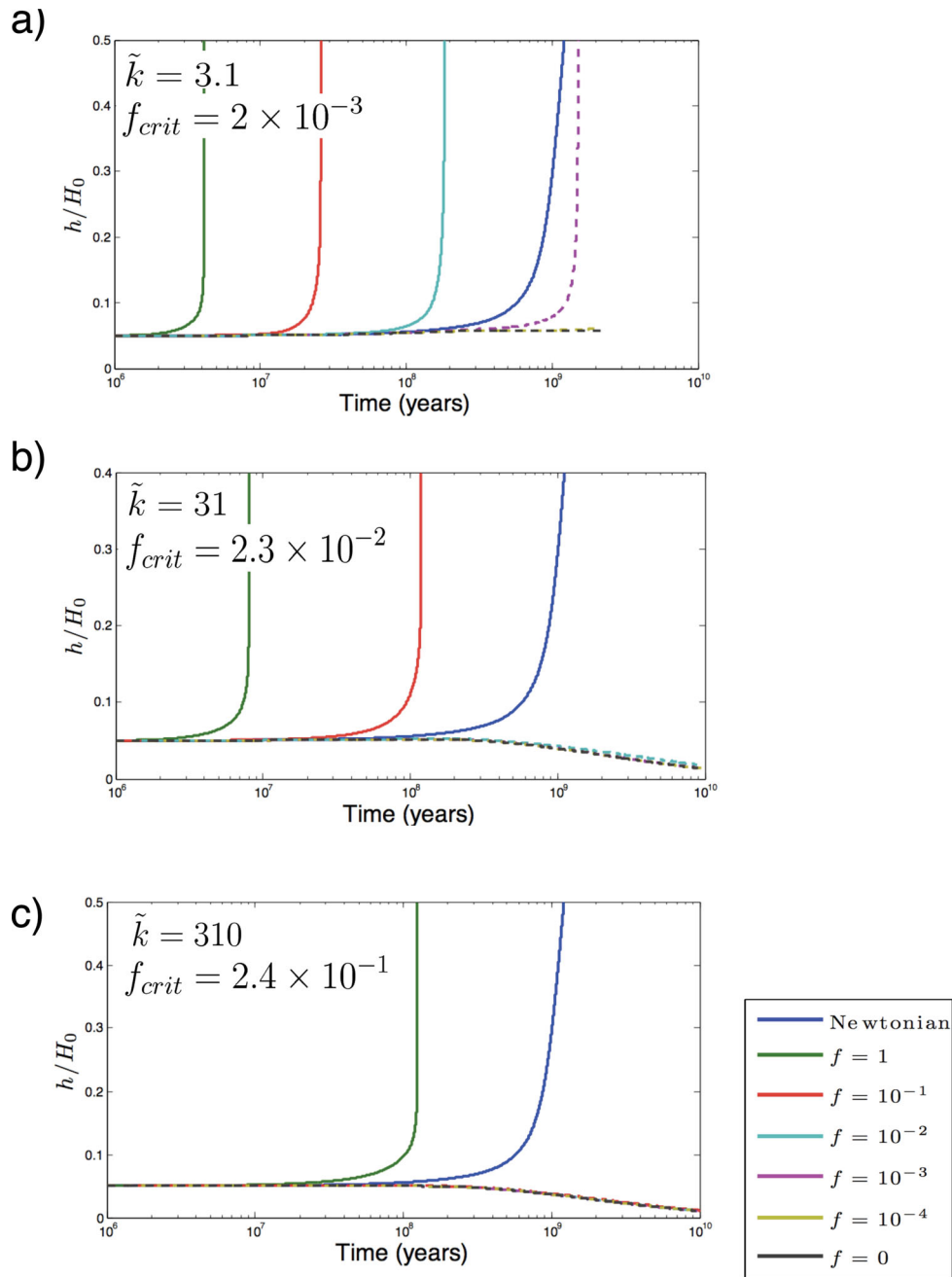


**Figure B1.** Perturbation amplitude as a function of time for the numerical model with  $\bar{\mu} = 10^3$ ,  $\lambda = 17.8H_0$ ,  $H_0 = 0.15D$ ,  $D = 2150$  km and  $Ra_0 = 10^6$ . When the perturbation amplitude equals  $0.5H_0$  a lithospheric drip instability has developed. Healing rate  $\tilde{k}$  is constant while  $f$  is varied between 0 and 1 for each plot. In all cases above  $\mathcal{R} = 3.3$ . The amplitude analysis is used to calculate  $\tilde{f}_{crit}$ , and it is converted to  $f_{crit}$  and shown on each plot. Only for cases where  $f > f_{crit}$  (solid lines) is perturbation growth enhanced relative to the Newtonian viscosity ( $f = \tilde{k} = 0$ ) shown in blue. Cases with  $f < f_{crit}$  are shown in dashed lines. For  $\tilde{k} = 3.1$  the  $f = 10^{-3}$  case does not decay although  $f < f_{crit}$ , however it does grow slower than the Newtonian case. All other cases with  $f < f_{crit}$  collapse down to the  $f = 0$ ,  $\tilde{k} \neq 0$  case (black line).